Omoniyi et al., J Material Sci Eng 2018, 7:5
DOI: 10.4172/2169-0022.1000485

Journal of Material Sciences & Engineering

Research Article Open Access

# Microstructural and Mechanical Properties of Spark Plasma Sintering of $Ni_{22}Cr_{11}Al$ Powders Synthesized by Mechanical Alloying for Thermal Barrier Coating

**Omoniyi FIS[1]*, Olubambi PA[2] and Sadiku RE[3]**

[1]College of Science, Engineering and Food Science, University College Cork Ireland
[2]Department of Chemical Engineering, University of Johannesburg, South Africa
[3]Department of Chemical, Metallurgical and Materials Engineering, Tshwane University of Technology, Private Mail Bag X-680, Pretoria, South Africa

## Abstract

Thermal barrier coatings (TBCs) systems are used to protect hot sections of industrial gas turbine blades against high temperature corrosion and oxidation.

Currently, MCrAlY powders up to 100 μm in diameter are used in the production of thermal barrier coatings by industrial gas turbine component manufacturers. It has been found that nanocrystalline MCrAlY layer provide better oxidation behaviour than currently used microstructure MCrAlY layer at elevated temperature.

In the present study, nanocrystalline $NI_{22}Cr_{11}Al$ composites was synthesized using high energy planetary ball milling for different periods of time, and the dense NI22Cr11Al alloy was fabricated by using spark plasma sintering process at different temperatures ranging from 1000°C to 1200°C. The resultant powder particles, bulk and dense samples were characterised using scanning electron microscope (SEM), X-ray diffraction analysis (XRD) and Micro Vickers hardness test. The results indicated that mechanical milling process produce morphology changes, particle size increase, crystallite size decrease down to nanometric level (40 nm) and formation of Nano dispersions in the process.

**Keywords:** Mechanical alloying; Mechanical properties; Microstructure; Spark plasma sintering; Thermal barrier coating

## Introduction

MCrAlY (M=Ni, Co) alloys typically find application as bond coat materials for the fabrication of thermal barrier coatings (TBCs)for Ni-super alloys-based gas turbine components to protect them when exposed to harsh oxidation environments [1,2].

Extensive research effort has been made in recent years for the development of MCrAlY alloys with improved high temperature performance properties, so that the service life of TBC could be extended [3-6].

In this regard profitable effects are observed when decreasing grain size in bond coat metal matrix and/or in presence of Nano sized dispersions of hard phase like oxides [7,8].

Mechanical alloying (MA) is one promising process use to produce Nano structured materials for plasma spray applications. It is a high energy ball milling process by which constituent powders are repeatedly deformed, fractured and welded by grinding media to form a homogeneous alloyed microstructure or uniformly dispersed particulates in a matrix [9]. The major process in MA for producing quality powders of alloys and compounds with well-controlled microstructure and morphology is the repeated welding, fracture, and re welding of the reactant mixed powders [10].

Ball to powder mass ratio or charge ratio (CR), milling time and rotational speed are the most significant and controllable process parameters, although other variables (milling device, atmosphere, process control agents, etc.) also affect the mechanical treatment outcome. Another important processing parameter is represented by the milling temperature [9]. The temperature of milling plays a vital role in deciding the constitution of the milled powder. Due to the fact that diffusion processes are involved in the formation of alloy phases irrespective of whether the final product phase is a solid solution, intermetallic, amorphous or nanostructure, it is anticipated that the temperature of milling will have a significant effect in any alloy system.

The application of a process control agent (PCA) eradicates the high possibility of contamination of the final powder product caused by recurrent collision that the powder withstands against the crushing bodies. And in the absence of process control agent, there is prevalence of fusing over the fractures which ensued in the production of hollow sphere-shaped particles up to millimeters in diameter.

The choice of a process control agent (PCA) hangs on the characteristic of the powder being milled and the purity of the final products.

The milling time is selected as to achieve a steady state between cold welding and fracturing of the powder particles [9]. The time needed vary depending on the kind of mill used, the intensity of the milling, the ball-to-powder ratio and the temperature of milling. However, it is paramount that the powder is milled just for the required time.

Spark plasma sintering (SPS) is a novel sintering technique with the characteristics of higher heating rate and shorter dwell times when

***Corresponding author:** Omoniyi FIS, College of Science, Engineering and Food Science, University College Cork Ireland, Tel: +353899801944; E-mail: folorunsoomoniyi@gmail.com

**Received** September 07, 2018; **Accepted** September 19, 2018; **Published** September 29, 2018

**Citation:** Omoniyi FIS, Olubambi PA, Sadiku RE (2018) Microstructural and Mechanical Properties of Spark Plasma Sintering of $Ni_{22}Cr_{11}Al$ Powders Synthesized by Mechanical Alloying for Thermal Barrier Coating. J Material Sci Eng 7: 485. doi: 10.4172/2169-0022.1000485

compared to conventional pressure-assisted sintering methods [11] which enhances sintering activity and leads to limited grain growth [12] During SPS, electrically conductive powders are subjected to a mechanical load and simultaneously crossed by an electric pulsed current to produce high local heating rates due to Joule effect. The emerging theme from the large majority of investigations of current activated sintering is that it has decided advantages over conventional methods including pressure less sintering, hot-pressing, and others. These advantages include: lower sintering temperature, shorter holding time, and marked comparative improvements in properties of materials consolidated by this method. Lower temperatures and shorter holding times have made it possible to sinter nanometric powders to near theoretical values with little grain growth [13].

The aim of this paper is to investigate the use of spark plasma sintering (SPS) as a rapid and efficient technique to evaluate possible benefits deriving from high energy ball milling of $NI_{22}Cr_{11}Al$ powders.

## Materials and Methods

### Feed stock powder and characterization

Commercial starting powders for coating were Ni (flow master metal powder 28/0.5-3.0 micron particle size 99.5%Ni), Cr (flow master metal powder, <10 micron particle size, 99.2%Cr) and Al (flow master metal powder<10 micron particle size, 99.7%Al) powders as bond coat. The elemental powders of Ni, Cr and Al were mixed together using the Tubular Shaker mixer T2F in mass ratio as shown in Table 1. Mixing speed of 72 rpm was chosen and a mixing time of 8 h was allowed. A 250 ml cylindrical plastic vessel with a fill level of 25% of powders loaded axially was used. The mixing vessel/container was placed in the mixing chamber and subjected to translational and rotational motion. And mixing was carried out in a dry environment at room temperature.

The MA process was conducted in a planetary ball mill (Retch PM400) using stainless steel containers and balls (2-5 mm diameter) at room temperature. The weight ratio of ball to powder was maintained at 10:1 and the ball milling was carried at a rotation rate of 250 rpm. Furthermore, the ball-milling was carried out for various times, namely 24 h, 30 h and 36 h using process control agent (PCA). Milling was interrupted after every 3 h for 10 mins to cool down the jar.

For the microstructure observations of the mixed powders and the milled, a small amount of the powder was mounted, and the cross sections of the powder particles were prepared by conventional metallographic techniques. Microstructure and chemical composition of different phases in the powders were studied employing Scanning electron microscope (SEM) with an energy dispersive spectrometer (EDS).

The XRD analysis was done to identify the phases present in the samples in Bruker $D_2$ Advanced diffractometer using cobalt as anode material at 30 Kv and 10 MA. The powders were scanned at a step scan mode of 0.02.

In addition, crystallite size evolution during mechanical milling was estimated from the line broadening of X-ray diffraction peaks using the Scherrer formula [14], i.e.

$$B(2\theta) = \frac{K\lambda}{L\cos\theta}$$

| Material | Ni | Cr | Al |
|---|---|---|---|
| NiCrAl | 67% | 22% | 11% |

**Table 1:** Chemical composition(in wt%) of NiCrAl mixed feedstock powder.

where,

B is peak width, that is inversely proportional to crystallite size (L),

ɵ is the Bragg angle,

k is the Scherrer constant which has been set equal to one, and

λ is the X-ray wavelength.

### Consolidation of the composites powders

In this work, the powders were consolidated by spark plasma sintering unit (H-HPD25-FCT System GmbH Germany). The powders were loaded into a graphite die 30 mm in diameter and poured into packs of thickness between 3 mm to 8 mm in which 5 mm was aimed at. A sheet of graphite foil was placed between the punch and the powders for easy sintered sample removal, thus prolonging tool life. In addition to this, the side walls as well as the top and bottom of the graphite die were coated with fine hBN slurry in order to limit the diffusion of carbon to the compacts.

A Pressure of 30 MPa was applied to die through hydraulic rams fixed to a press. The current pulse of 3.3 ms fixed was generated by the power supply in which each pulse sequence contains 12 pulses was used. Temperature was measured by infra-red pyrometer to obtain a true value of temperature during consolidation. The densification process was carried out using a multistep heating method with heating rate of 100°C/min from room temperature to 1000°C, 1100°C and 1200°C.at dwell time of 3 mins and a holding time of 1 min at 600°C were involved.

### Characterization of the sintered samples

The Sintered bulk surface were cleaned by grinding the surface using (Saphir 520 grinding machine made in Germany) with SiC P320 paper at speed 150 micron/min and a force of 25 N for 30 mins. It was polished using both Aka-largan with diameter max 9 µm poly and Aka-napal with doublo 1 µm poly to remove diffused carbon. The densities of the sintered polished samples were performed by water displacement method (Archimedes principle process) using OHAUS density scale weighing balance of 0.001 mg accuracy. The density of the best sintered samples was 98.99% of the theoretical density.

Micro-hardness was measured using Vickers micro hardness tester (Future-Tech Corporation Tokyo- Japan) under the load of 25 kgf for a dwell time of 10 secs. For the load, five indents were made of which the average values were calculated.

## Results and Discussion

### Feedstock powder characterization

The XRD pattern of the as-mixed (un-milled) elemental powders and theNi-22Cr-11Al powder ball-milled for different times are shown in Figure 1.

The initial powder mixture consists of the elemental metals of Ni, Cr and Al.

After 24 h, 30 h and 36 h ball-milling, the intensity of the peaks show some significant change. The sharp peaks from the crystalline elements of Ni, Cr and Al have disappeared as seen in Figure 1. This is due to the grain size reduction and/or accumulation of mechanical strains.

Peak broadening and reduction in intensity of diffraction peaks of ball-milled powders are associated with the refinement in crystallite size, lattice internal strains and instrumental effects [15].

The formation of FCC γ/γ' Ni- Phase after 36 h ball-milling can be attributed to the dissolution of the alloying elements in the Ni lattice.

However, the disappearance of Al and Cr peaks can mainly be associated with formation of Nickel solid solution.

The SEM morphology of the blended Ni-22Cr-11Al is shown in Figure 2a. Mechanical mixing of the powders occurred characterized by smooth and spherical particles. Powder particles did undergo changes as the milling times increases as shown in Figure 2b-2d. The significant change in the powder morphology caused by MA is apparent, more specifically the smooth particles became gradually rough, irregular and flake-like shaped a consequence of balling-milling operation. The particles after the ball-milling time of 24 h had collided sufficiently with the balls, work hardened and agglomerated. The agglomeration of the powders is mostly due increase resistance to fracture and strong tendency of cohesion between particles with decreasing particle size.

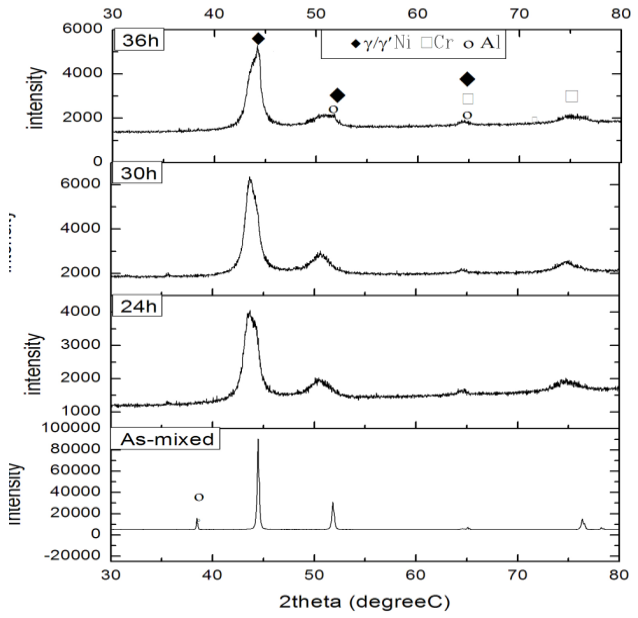


**Figure 1:** XRD pattern of the as-mixed (un-milled) elemental powders and the Ni-22Cr-11Al ball-milled powders for 24 h, 30 h and 36 h.

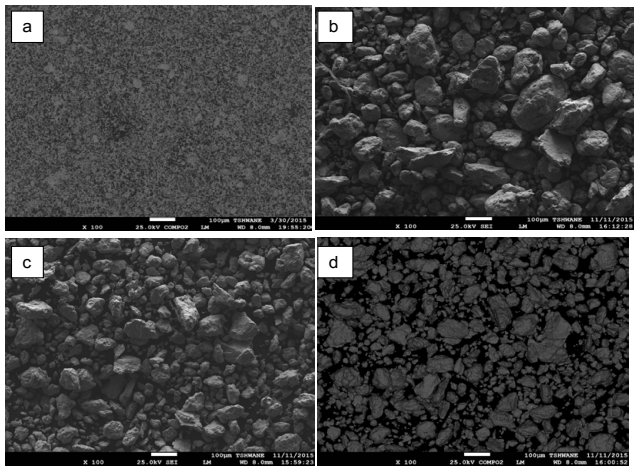


**Figure 2:** SEM Micrographs of the as-mixed (un-milled) elemental powders and the Ni-22Cr-11Al ball-milled for 24 h, 30 h and 36 h as in (a), (b), (c) and (d) respectively.

After ball-milling for 30 h, majority of the particles showed relatively smaller size compared to that particles ball-milled for 24 h. The presence of rough, irregular and flaky particles is a indicative of micro forging and cold welding event predominance over fracturing. As seen in Figure 2d, the morphology and size of powders drastically changed after 36 h ball-milling and the powders exhibited a considerable smaller size and finer particles than the powders ball-milled for 24 h and 30 h due to increase in particle-particle contact and increase in surface area of the milled powder particles.

As a result of the work hardening effect and high density of defects such as dislocations and vacancies for long ball-milling times, the fracture and welding of powders reach an equilibrium state. However, due to the higher bonding strength of the finer particle size, the ability of particles to stand further plastic deformation is decreased and a higher force is required to fracture the small particles during the ball-milling process [16].

To provide some quantitative, albeit approximated values of the average crystallite size under the different ball-milling conditions examined. Figure 3 shows the results obtained according to Scherrer formula. The average crystallite size decreased down to nanometric level of about 40 nm after ball milling. The amount of powder recovered from the container at different ball-milling times is plotted in Figure 4. It is obvious that an increase in the ball-milling time lead to a decrease in the powder yield. About 75% of the powder was recovered after ball-milling for 24 h. By increasing the ball-milling time to 30 h, a lower portion of 60% of the powder was recovered from the container. When the ball-milling time increased to 36 h, only a lower powder yield of about 45% was obtained. At this point, a large amount of powder remained in the grinding media as evidenced by a relatively thick layer of powder over the balls and the inner wall of the container. Basically, due to the frequent mechanical impact of the balls on the powder particle, part of the milled powders is cold-welded over the grinding media, forming a coating layer [16,17].

The content of contamination in the bulk Ni-22Cr-11Al alloy samples made from the powders ball-milled for various ball-milling times is given in Table 2. The results indicated the increase of ball milling time leads to a noticeable contamination of oxygen in the bulk

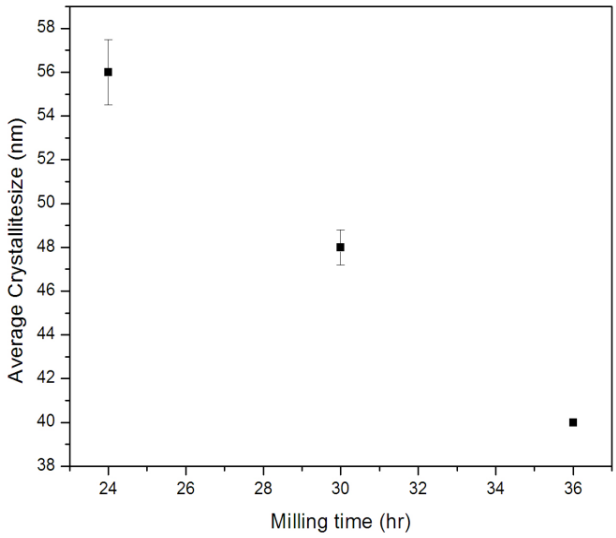


**Figure 3:** Crystallite size (scherrer formula) of Ni-22Cr-11Al powders as a function of ball-milling time.

samples. The contaminations can be traced to the milling atmosphere and chemical purity of the starting powder. It is also notable that the long ball-milling times also resulted in increased contamination of Fe and C.

The Fe and C contaminations are from the wear of the stainless-steel milling balls and containers during the milling process. The increase in content of contamination with ball-milling time is a common problem with the MA technique. In fact, an argon atmosphere is incapable of reducing the oxygen partial pressure sufficiently and it is practically impossible to prevent the surrounding atmosphere from leaking into the milling container during the MA [18,19]. Figure 5 indicates the results of EDS analysis performed on Ni22Cr11Al powders after ball-milling. The graph revealed convincingly that oxygen concentration has increased from 0.2% to 7%. And the concentration of Al went up from 11% to 19% while the concentration of Cr and Ni showed no substantial increase i.e. concentration almost of the same amount.

## Sintering behaviours of the mixed and ball-milled powders during spark plasma sintering

During the SPS process, the powder particles were subjected to compression between top/bottom punches and the die wall. It is possible to obtain the displacement (shrinkage) or displacement rate data of punch as a function of time or temperature during sintering [20]. The relative piston travel (displacement) can be used as an indirect measure of densification during spark plasma sintering. And displacement towards negative or positive direction could mean expansion or shrinkage respectively [21].

| Ball-milling (hr) | 02 contamination (wt%) | Fe contamination (wt%) | C contamination (wt%) |
|---|---|---|---|
| 24 | 2.55 | 0.01 | 0.30 |
| 30 | 3.15 | 0.01 | 0.40 |
| 36 | 3.75 | 0.02 | 0.45 |

**Table 2:** The content of contamination in bulk of Ni-22Cr-11Al made from various ball milling times.

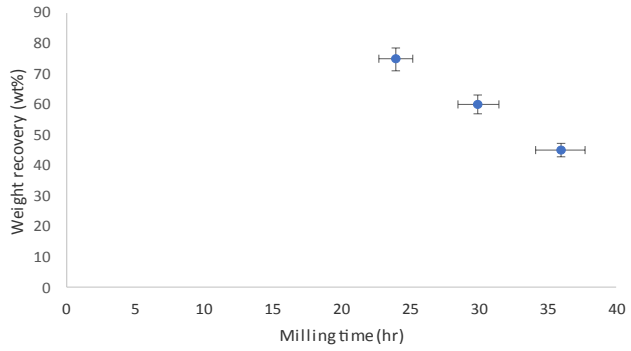


**Figure 4:** The amount of powder recovered from the milling container as a function of ball-milling time.

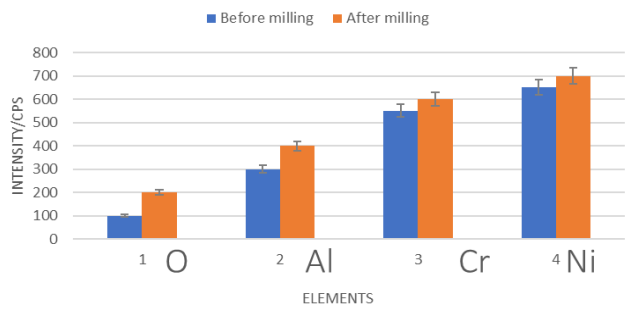


**Figure 5:** The concentration increments of Oxygen and Aluminium after 36 h ball-milling.

Ni22Cr11Al bulk samples were successfully sintered at 1000°C, 1100°C and 1200°C with a dwell time of 3 mins respectively and a holding time of 1 min at 600°C under a pressure of 30 MPa. The typical displacement (shrinkage) and time versus temperature plots obtained during sintering of the compacts are presented in Figures 6 and 7.

The characteristic plot obtained for each compact pertaining to particular sintering temperature can be related to the mechanisms of densification of the powder particles. Such analysis was reported in literature for identifying the densification mechanisms of the powder particles during SPS process [22].

In the present study, three main stages can be identified for the displacement variations which are the first 3 mins to 5 mins, when pressure is increasing, and the powder is compressed as a green body. The next point is the flat stage then sintering which occurred at the final stage as the temperature reaches 800°C to 950°C.

It can be seen from Figures 6 and 7 that the maximum displacement of the powder particles that took place are 6.5 mm and 2.5 mm for as-mixed (un-milled) and milled alloy respectively. The change in displacement is determined by the consolidation behavior of green body and thermal expansion of the dense body [23].

Also, it was found that powder consolidation was progressively promoted in milled powders compared to as in un-milled powders. Moreover, powders subjected to extensive mechanical milling underwent severe strain hardening and strong reduction of the crystallite size, allowing Nano structuring and increased powder sinter ability. Thus, sintering ability of the ball-milled powder is higher than that exhibited by the un-milled powders consistently with the consolidation dynamics displayed by the same systems.

## Characterization of microstructure, density and micro hardness

The SEM microstructures of samples obtained by SPS starting from unmilled powders to 36 h ball-milled at 1000°C, 1100°C and 1200°C exhibited different microstructural variations within the compacts shown in Figures 8 and 9.

Considering both un-milled and ball-milled powders at the optimal sintering temperature of 1200°C when 36 h ball-milled powders was used, Archimedes measurement indicated the achievement of best densification as seen in Figure 9c, while some residual porosity were still present in the bulk material sintered at 1000°C and 1100°C for both powder samples in Figures 8 and 9. It was evidenced in Figure 9c, that porosity is almost completely eliminated. Moreover, it was observed that there were increase in density of the compacts with increase in sintering temperature.

Two phased microstructure were also present at examined bulk products obtained from both Unmilled and ball-milled powders. For all temperatures of sintered samples, the microstructure were mainly composed of two phases, identified as in dark grey and light grey. Based on the EDS analysis as shown in Figure 10 and the XRD diffraction results carried on the starting powders (Figure 1), it is possible to assess that the darker region corresponds to the Al-rich β phase while the

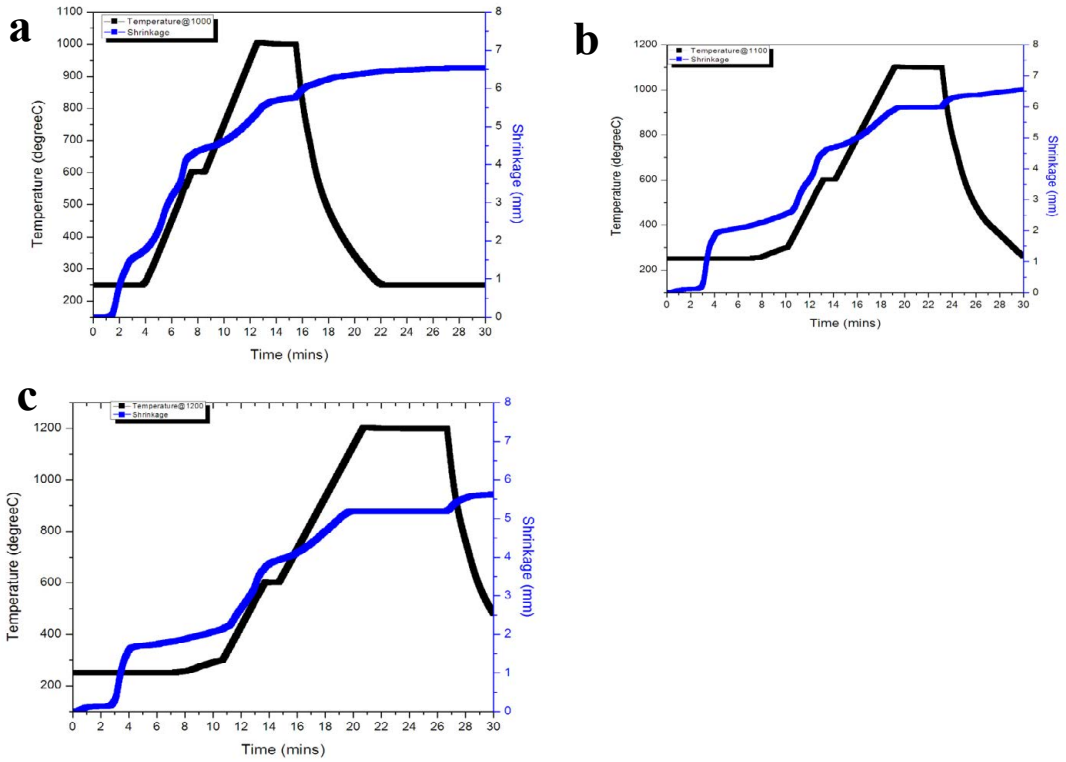


**Figure 6:** Shrinkage (displacement) and temperature curves of un-milled powder for S-1000 (a), S-1100 (b) and S-1200 (c).

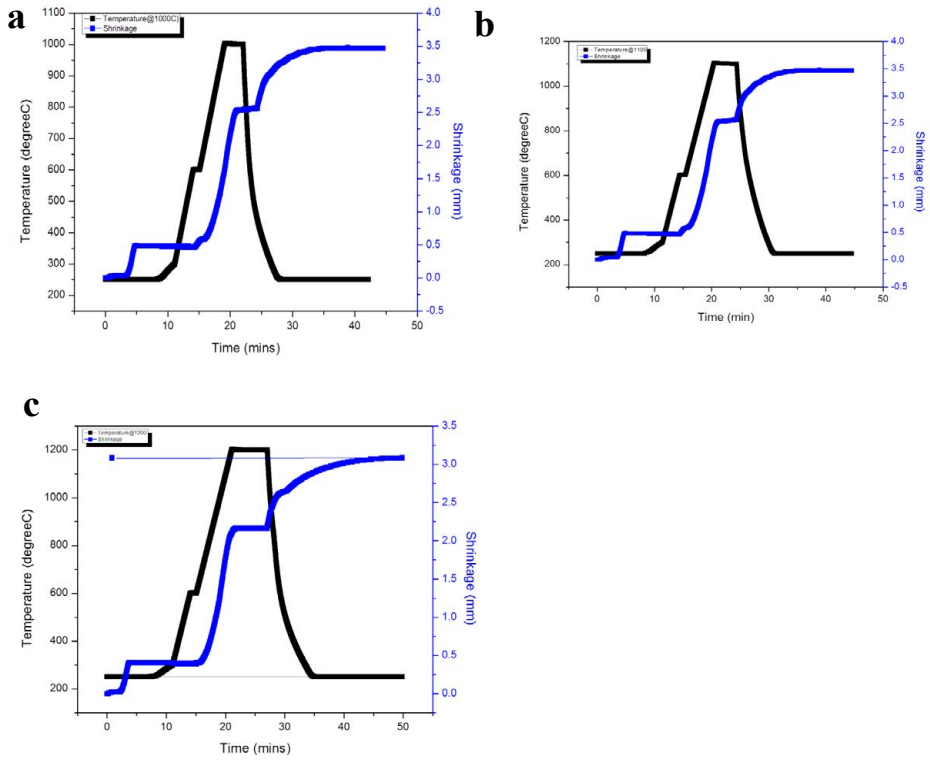


**Figure 7:** Shrinkage (displacement) and temperature curves of 36 h ball- milled powder for S-1000 (a), S-1100 (b) and S-1200 (c).

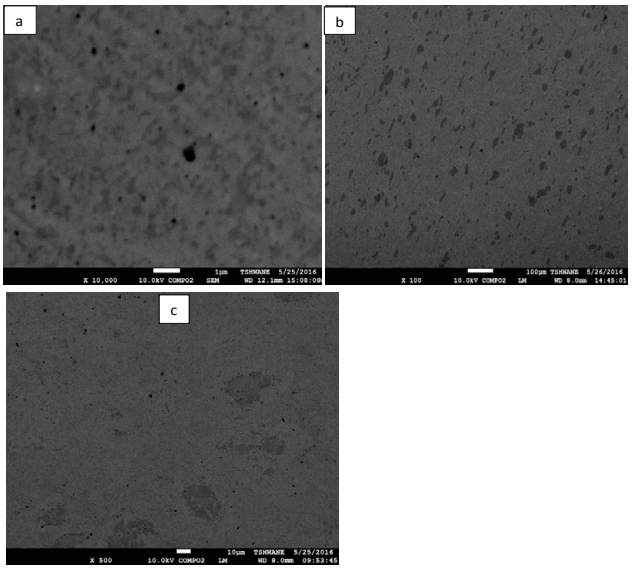


**Figure 8:** SEM micrographs of SPS compacts for un-milled powders at 1000°C (a), 1100°C (b) and 1200°C (c).

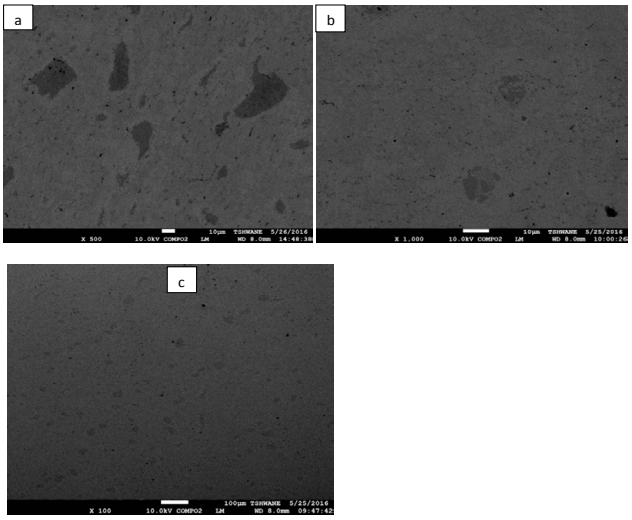


**Figure 9:** SEM micrographs of SPS compacts for 36 h ball-milled powders at 1000°C (a), 1100°C (b) and 1200°C (c).

lighter continious region contains γ/γ' phase.

Nevertheless, it is apparent that the relative coaser microstructure of the Un-milled samples becomes progressively finer when ball-milling process is performed before sintering. The microstructure refinement obsevered in bulk material Figures 9a-9c is directly originated from ball-milling process received by the powder before sintering. A detailed view of Figure 9c where ball-milling was prolonged for 36 h, can be clearly seen that the distribution of the two phases resulted in submicrometer level and these observation can be justified on the basis of the characteristics of ball-milled powders sintered by SPS.

The XRD pattern of 36 h ball-milled NI-22Cr-11Al powder obtained before and after SPS-consolidation at 1200°C shown in Figure 11 confirmed the presence of γ'-$NiAl_3$ and γ-NiCrAl phases in powder particles and as well as in the compact. The relatively peaks narrowing

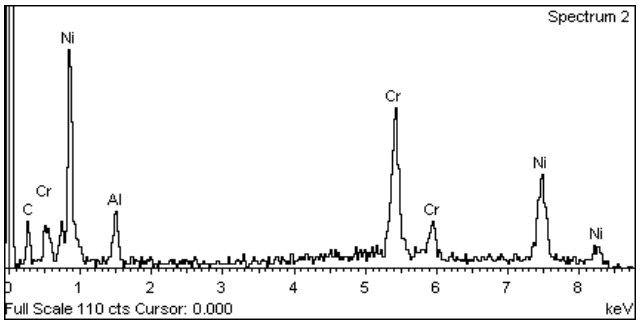


**Figure 10:** EDS analysis performed on the bulk sample obtained by SPS at 1200°C.

| Sample | Temperature (°C) | Relative density (%) |
|---|---|---|
| As-mixed | 1000 | 94.89 |
| 36 h milled | 1000 | 96.78 |
| As-mixed | 1100 | 95.65 |
| 36 h milled | 1100 | 97.20 |
| As-mixed | 1200 | 97.97 |
| 36 h milled | 1200 | 98.99 |

**Table 3:** Results of density of sintered samples.

clearly seen can be attributed to certain grain growth occuring during the consolidation process.

Table 3 summarized the results of relative density of the sintered as-mixed (unmilled) and 36 h ball-milled Ni-22Cr-11Al samples. Density values of the sintered Ni22Cr11Al sample showed that the material is dense which indicates low porosity and voids. The relative density above 98% was obtained for 36 h ball-milled sample SPS at 1200°C. And the overall results of the density measurement revealed that there is an obvious increase in the density of the compacts with increase in sintering temperature as shown in Figure 12. The reason is as a result of improved bonding between the constituent elements due to high temperature attained in contact area, over the melting temperature of the material leading to localized melting which enhances interparticle bonding. Density is mass per unit volume.

Density of Ni=8.908 g/cm$^3$, Cr=7.19 g/cm$^3$, Al=2.7 g/cm$^3$.

The density of the sintered grinded and polished bodies was determined by Archimedes principle using the density determination kit of OHAUS density scale. The Principle states that every solid body immersed in a fluid loss weight by an amount equal to that of the fluid it displaces.

$$\text{Density } (Q) = A/(A-B) \times Q_0$$

A is weight of solid in air

B is weight of solid in water

$Q_0$ is the density of water=1.006 g/cm$^3$.

The Vickers hardness was measured randomly at five different locations for the sintered samples surface and average values were presented in Table 4.

Figure 13 shows the influence of densification on micro hardness of samples at different sintering temperature. The lowest hardness belonged to sample made from the blended powder mixture sintered at 1000°C showing the value of 287 ± 1.8 $HV_{0.025}$ and the highest hardness value belonged to sample made from powders ball-milled

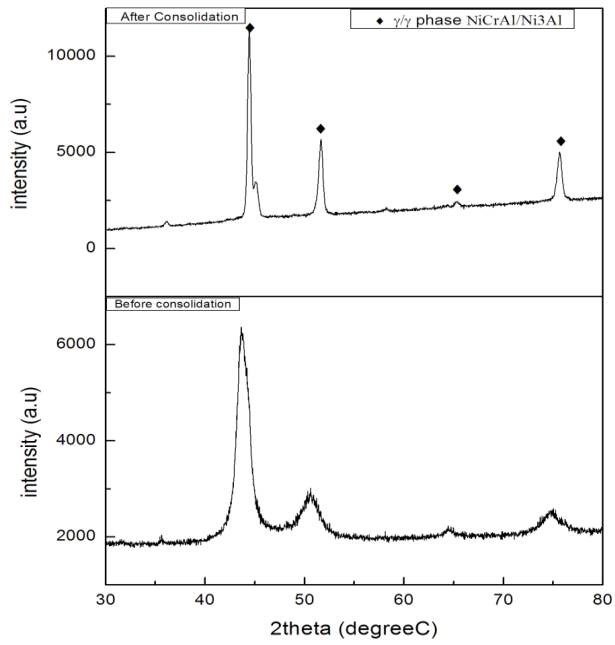


**Figure 11:** Comparison of XRD pattern of 36 h ball-milled Ni-22Cr-11Al powders before and after consolidation at 1200°C.

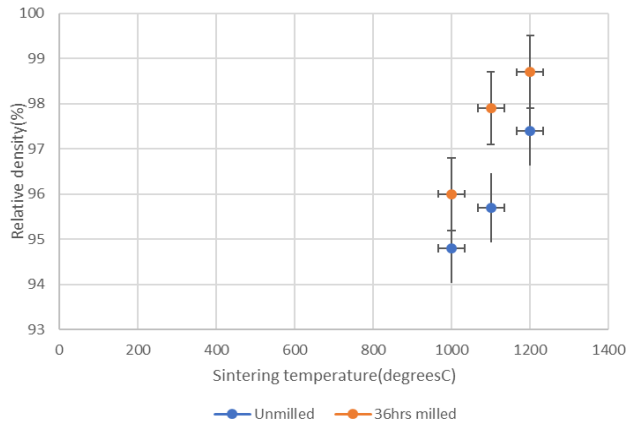


**Figure 12:** Effect of sintering temperature on the relative density of NI-22Cr-Al as-mixed (un-milled) and 36 h ball-milled samples obtained SPS.

| Sample | Temperature (ºC) | Relative density (%) |
|---|---|---|
| As-mixed | 1000 | 287 ± 1.8 |
| 36h milled | 1000 | 355 ± 1.6 |
| As-mixed | 1100 | 300 ± 2.0 |
| 36h milled | 1100 | 467 ± 2.2 |
| As-mixed | 1200 | 420 ± 2.4 |
| 36h milled | 1200 | 596 ± 2.8 |

**Table 4:** Results of Micro hardness of sintered samples.

for 36 h sintered at 1200°C of the value 596 ± 2.8$HV_{0.025.}$ A progressive increase in hardness of the Ni-22Cr-11Al alloy made from the 36 h ball-milled compared to the as-mixed could be put down to crystallite size refinement, work hardening of the powders and solid solution strengthening. Furthermore, the results of the hardness measurement revealed that the sample with highest densification gives the highest

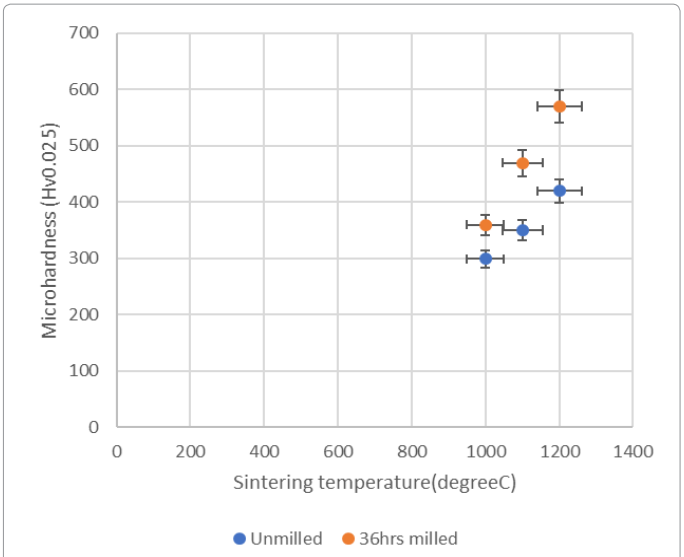


**Figure 13:** Vickers hardness of the as-mixed (un-milled) and 36 h ball-milled SPS compacts as a function of sintering temperature.

hardness values. The microstructure contribution to the high observed increase in hardness could be attributed to progressive high sintering density [24]

F=Load in kgf

d=Arithmetic mean of the diagonals d1 and d2 in mm.

Hv=Vickers hardness (to MPa multiply by 9.807 and to GPa multiply by 0.001.

## Conclusion

An investigation based on mechanical alloying and Spark Plasma Sintering processing of Ni-22Cr-11Al (wt%) powders was performed in this research.

The Characteristic of both powders and corresponding sintered samples were found significantly affected by the milling treatment received.

Morphology, Crystallite size decreases and Particle size increase were the vital features evidenced after mechanical alloying.

The effect of ball-milling times on the structural characteristic of the powders, bulk and dense Ni-22Cr-11Al alloy after 36 h lead to bulk product microstructure becoming progressively finer with respect to γ (NiCrAl)/γ' ($Ni_3Al$) phases which are finely distributed throughout the whole bulk sample. However, increase in ball-milling time also resulted to increase in the quantity of contamination introduced by the grinding media and milling atmosphere.

The sintering temperature has a profound influence on the densification, microstructure and mechanical properties. The SPS-consolidation carried out at 1200°C for 36 h ball-milled revealed denser and more uniformly distribution of phase.

Hardness values have great influence from sintering temperature for both samples nanostructured and conventional. The hardness of bulk samples showed a decidedly upward trend with an increase in ball-milling time. Hence the highest hardness value was exhibited for samples produced from 36 h ball-milled at 1200°C since the

microstructure was characterised by fine distribution of precipitates and complete metallurgical bonding.

Thus, the SPS information, XRD pattern and microstructure images revealed that bulk deformation and particle rearrangement depends on the size of the powder particles used for consolidation.

It is then obvious that SPS process appears to be a promising technique to rapidly produce dense sample alloys with refined microstructure, and such as ensuring rapid turn-over and low cost in high temperature applications.

## References

1. Sahoo P, Carr T, Martin R, Dinh F (1998) Thermal spray manufacturing issues in coating IGT hot section components. J Therm Spray Technol 7: 481-483.
2. Barbezat G, Refke A, Vetter J, Nestler M (2007) Surface solutions for the requirements of tomorrow. Sulzer Technical Review 4225.
3. Tang F, Ajdelsztajn L, Schoenung JM (2004) Influence of cryomilling on themorphology of the oxide scales formed on HVOF CoNiCrAlY coatings. Oxid Met 61: 219-238.
4. Tang F, Ajdelsztajn L, Kim GE, Provenzano V, Schoenung JM (2004) Effects of surface oxidation during HVOF processing on the primary stage oxidation of a CoNiCrAlY coating. Surf Coat Technol 185: 228-233.
5. Young DJ (2008) High temperature oxidation and corrosion of metals (Vol. 1). Elsevier.
6. Schoenung JM, Tang F, Ajdelsztajn L, Kim GE, Provenzano V (2005) Processing and characterization of thermal barrier coatings with cryomilled bond coats. Mater Forum 29: 414-419.
7. Zhang Q, Li CJ, Li CX, Yang GJ, Lui SC (2008) Study of oxidation behavior of nanostructured NiCrAlY bondcoatings deposited by cold spraying. J Surf Coat Technol 202: 3378-3384.
8. Kim GE, Addona T, Richer P, Jodoin B, Al-Mathami A, Brochu M (2010) Characterization and Evaluation ofNanostructured Bond Coats from Non-Cryogenically Milled Feedstock. J Therm Spray Technol 112: 29-33
9. Suryanarayana C (2001) Mechanical alloying and milling. Progress in Materials Science 46: 1-184.
10. Benjamin JS (1992) Mechanical alloying- history and future potential. Adv Powder Metall Part Mater 7: 155-168.
11. Li W, Gao L (2003) Fabrication of HAp-ZrO2 (3Y) nano-composite by SPS. Biomaterials 24: 937-940.
12. Licheri R, Orrù R, Musa C, Cao G (2008) Combination of SHS and SPS Techniques for fabrication of fully dense ZrB2-ZrC-SiC composites. Mater Lett 62: 432-435.
13. Courat A, Molenat G, Galy J, Thomas M (2008) Microstructures and mechanical properties of TiAl alloys consolidated by spark plasma sintering. Intermetallics 16: 1134- 1141.
14. Langford JI, Wilson AJC (1978) Scherrer after sixty years: a survey and some new results in the determination of crystallite size. J Appl Crystallogr 11: 102-113.
15. Klug HP, Alexander LE (1974) X-ray Diffraction Procedures. John Wiley & Sons, New York pp: 643
16. Kobayashi K (1995) Formation of coating film on milling balls for mechanical alloying. Mater Trans, JIM 36: 134-137.
17. Takacs L, Torosyan AR (2007) Surface mechanical alloying of an aluminum plate. J Alloys Compd 434: 686-688.
18. Singer RF, Oliver WC, Nix WD (1980) Identification of dispersoid phases created in aluminum during mechanical alloying. Metal Trans A 11: 1895-1901.
19. Li C, Liang B (2008) Study on the mechanochemical oxidation of ilmenite. J Alloys Compd 459: 354-361.
20. Devaraj S, Sankarany S, Kumar R (2013) Influence of spark plasma sintering temperature on the densification, microstructure and mechanical properties of Al-4.5 wt.% Cu alloy. Acta Metall Sin (Engl. Lett.) 26: 761-771.
21. Hu Q, Luo P, Yan Y (2008) Influence of spark plasma sintering temperature on sintering behavior and microstructures of dense bulk $MoSi_2$. J Alloys Compd 459: 163-168.
22. Diouf S, Molinari A (2012) Densification mechanisms in spark plasma sintering: Effect of particle size and pressure. Powder Technol 221: 220-227.
23. Licheri R, Fadda S, Orrù R, Cao G, Buscaglia V (2007) Self-propagating high-temperature synthesis of barium titanate and subsequent densification by spark plasma sintering (SPS). J Eur Ceram Soc 27: 2245-2253.
24. Lee KM, Oh DK, Choi WS, Weissgärber T, Kieback B (2007) Thermomechanical properties of AlN-Cu composite materials prepared by solid state processing. J Alloys Compd 434: 375-377.